



Eidgenössische Technische Hochschule Zürich
Swiss Federal Institute of Technology Zurich

Simulation of Quantum Dots

Group project

Laboratory for Nanoelectronics

Prof. Dr. Vanessa Wood

Integrated Systems Laboratory

Department of Information Technology & Electrical Engineering
ETH Zurich

Handed in by

Christian Funck & Matthias Dittberner

Date

June 6, 2013

Supervisors: Prof. Dr. Vanessa Wood
Prof. Dr. Mathieu Luisier

Christian Funck
Plattenstrasse 71
8032 Zurich
09-920-177
cfunck@student.ethz.ch

Matthias Dittberner
Luegislandstrasse 269
8051 Zurich
09-913-450
mdittber@student.ethz.ch

Contents

| | | |
|-----------------------------------|---|-----------|
| 1 | The Quantum Dot | 1 |
| 2 | Colloidal Nanocrystal Synthesis | 5 |
| 2.1 | The synthesis | 5 |
| 2.2 | Reaction conditions | 6 |
| 3 | QD Solar Cells | 7 |
| 3.1 | Solar Cell Principles | 7 |
| 3.2 | Solar Cells using QDs | 8 |
| 3.2.1 | Example of a PbS QD Solar Cell | 9 |
| 4 | Analysis of PbS QD simulation data | 11 |
| 4.1 | Energy levels | 11 |
| 4.2 | Band gap | 12 |
| 4.2.1 | Band gap of QDs in presence of an applied voltage | 13 |
| 4.3 | Wave functions | 13 |
| 4.3.1 | Shape of the wave functions | 13 |
| 4.3.2 | Influence of an electric field | 18 |
| 4.4 | Conclusions | 19 |
| A | Lead sulfide (PbS) parameters | 21 |
| A.1 | Basic characteristics | 21 |
| A.2 | Tight binding parameters | 21 |
| Declaration of Originality | | 23 |
| Index | | 23 |
| Bibliography | | 23 |

Acknowledgements

We would like to thank our supervisors Prof. Dr. Wood and Prof. Dr. Luisier for giving us the opportunity to carry out this group project and giving us a first insight into the highly interesting field of nanoelectronics.

Further, we would like to thank Olessya Yarema, PhD student at the Laboratory for Nanoelectronics, for showing us nanocrystal synthesis in the laboratory and providing us with experimental data.

We are also very thankful to Deniz Bozyigit, PhD student at the Laboratory for Nanoelectronics, for his help and reading materials.

Abstract

In this group project, we made ourselves acquainted with the subject of quantum dots (QD) and QD solar cells as an application thereof.

We used OMEN, a simulation tool for nanoelectronic devices, for simulating lead sulfide (PbS) QDs. We created a MATLAB toolbox which simplifies the simulation as well as the administration and visualisation of simulation data significantly.

We then simulated the eigenenergies and eigenstates of PbS QDs for different parameters and analyzed the data. In particular, the dependence on the QD's size and on the electric field were investigated. In the case of band gaps, we compared the results with experimental absorption data.

During the project, we also had the possibility to observed nanocrystal synthesis in the laboratory.

Chapter 1

The Quantum Dot

Quantum dots are atomic structures (usually spherical) that have a size of about 1-10nm in diameter. They are often referred to as nanocrystals (NCs), though this term is more general and includes also other shapes and morphologies, which might extend to several μm , such as rods, wires etc. Figure 1.1 gives some examples of possible shapes and morphologies, that are possible with nowadays technologies.

Quantum Dots (QDs) are possible with various materials such as metals, semiconductors and compounds. According to their size and material, a QD can contain just a few or millions of atoms. A 10nm cube of GaAs contains for example 40,000 atoms [SalehTeich].

The properties of QDs are strongly dependent on their size. Figure 1.3 illustrates this effect for a semiconductor QD. Under ultraviolet excitation, the QDs emit light according to their size and therefore band gap.

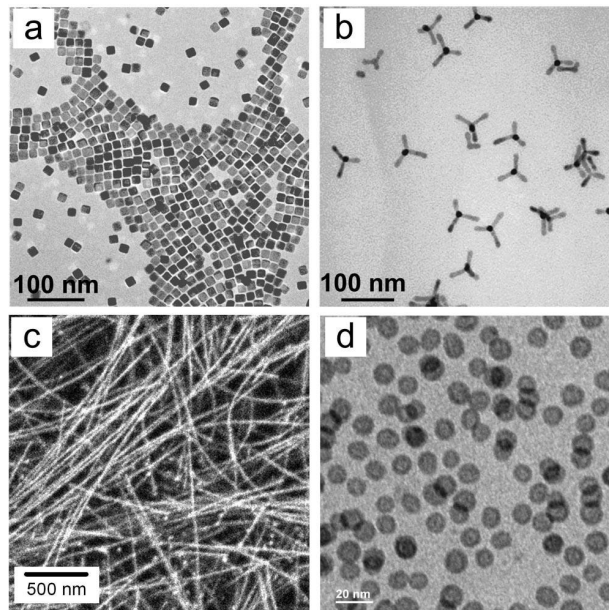


Figure 1.1: Examples of inorganic nanomaterials with different shapes and morphologies synthesized by colloidal chemistry: (a) PbSe cubes; (b) CdTe tetrapods; (c) PbSe nanowires and (d) hollow iron oxide nanoparticles. SOURCE: [Talapin]

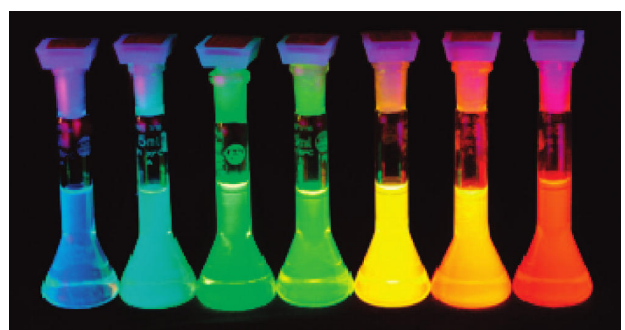


Figure 1.2: This photograph shows the size-dependent PL of the quantum dots. The particles with the smallest ($\sim 1.7\text{nm}$) CdSe cores emit blue and those with the largest cores ($\sim 5\text{nm}$) emit red. SOURCE: [Talapin]

Basic physics of the Quantum Dot For bulk materials the band gap is a fixed parameter, that specifies the type of material. But when a particle gets smaller and reaches a size of about 10nm this will not be the case anymore. The band gap is then depending on the size of this particle (NCs). As the mobility of the charge carriers (electrons, holes) is very limited in all three dimensions in the quantum dot, the energy levels are not continuous, but instead discrete. This phenomenon is called the *quantum size effect*.

The band gap of a spherical QD of radius R is then approximately:

$$E_g \approx E_{g,0} + \frac{\hbar^2 \pi^2}{2m_{eh} R^2} \quad (1.1)$$

where $E_{g,0}$ denotes the band gap of the bulk material and m_{eh} is obtained through the effective masses of electrons and holes $m_{e,p}$:

$$m_{eh} = \frac{m_e m_h}{m_e + m_h} \quad (1.2)$$

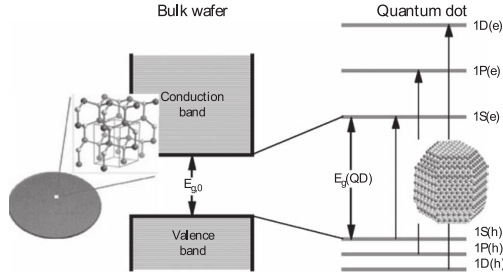


Figure 1.3: The left illustration shows the band structure of a bulk semiconductor with energy band gap $E_{g,0}$, whereas the the right one illustrates the discrete energy levels of a QD and its energy gap $E_g(QD)$. SOURCE: [Klimov]

We will see later in chapter 4.2 that the QD absorption spectrum as shown in figure 1.3(c) is not really discrete; as it is not possible to fabricate QDs that are perfectly equal in size, this results in a broadening of the spectrum. The energy gap increases for decreasing QD sizes, because more energy is required to confine the electron to a smaller volume. This is caused by Heisenberg's uncertainty principle , which says, that if we want to locate a particle of effective mass m (for example an electron), on an x-axis within an interval Δx , we can only make an uncertain prediction of its impulse. If the spatial region gets smaller, the uncertainty of the impulse will increase.

$$\Delta p_x \sim \frac{\hbar}{\Delta x} \quad (1.3)$$

This adds to the kinetic energy of the free particle, which is called the confinement energy , that has an significant impact, if it gets bigger than the thermal energy of the particle.

$$E_{confinement} = \frac{(\Delta p_x)^2}{2m} \sim \frac{\hbar^2}{2m(\Delta x)^2} > \frac{1}{2}k_B T \quad (1.4)$$

From this we can conclude, that the quantum size effect is relevant if

$$\Delta x < \sqrt{\frac{\hbar^2}{mk_B T}} \quad (1.5)$$

Table 1.1 shows 4 possible confinement structures, which are illustrated in Figure 1.4 with their characteristic energy levels in the conduction band.

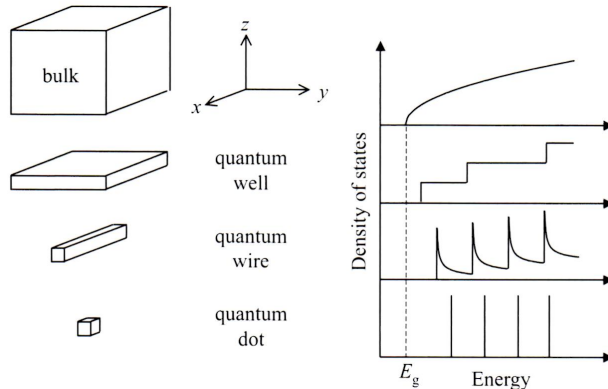


Figure 1.4: Schematic representation of quantum wells, wires and dots (left). The generic shape of the density of states function for electrons in the conduction band of a semiconductor with band gap E_g is shown for each type of the structure (right). SOURCE: [Fox]

| Structure | Quantum confinement | # of free dimensions | Electron density of states |
|---------------------------|---------------------|----------------------|----------------------------|
| Bulk | none | 3 | $\propto E^{1/2}$ |
| Quantum well/superlattice | 1-D | 2 | $\propto E^0$ |
| Quantum wire | 2-D | 1 | $\propto E^{-1/2}$ |
| Quantum dot/box | 3-D | 0 | discrete |

Table 1.1: Number of degrees of freedom tabulated against the dimensionality of the quantum confinement. The final column shows the functional form of the density of states for free electrons. SOURCE: [Fox]

Fabrication techniques of QD A lot of different ways to make QDs have been developed. Research efforts are made to create more efficient QDs and new shapes and morphologies. As QDs are more and more interesting for various commercial applications, low costs play an important factor. The colloidal chemistry has made a major contribution, as it offers low energy synthesis of NCs/QDs using very simple and affordable laboratory equipment. In the next chapter we will briefly discuss the mentioned technique, by giving a short overview that avoids the use of chemical terms as much as possible, rather than a detailed disquisition, as this is a research field on its own.

Some other methods are listed below.

Physical methods

Molecular-beam-epitaxy (MBE)
Metalorganic-chemical-vapor-decomposition (MOCVD)
Vapor-liquid-solid (VLS)
Electron-beam lithography

Characterization

High-energy-input, expensive apparatus, used for QDs
High-energy-input, used for QDs
High-energy-input, used for quantum wires

Chemical methods

Colloidal chemical synthesis of crystalline semiconductor nanoparticles

Characterization

Low-energy-input, wet chemistry, used for various structures

Applications In biology and chemistry QDs are used as spectral tags that are attached to molecules, making their position visible for identification under optical illumination. In the past, one used organic dyes, but compared to QDs the sharpness of emission lines is not as good.

In electronics, QDs are used to increase the efficiency of lasers [SemiconductorCD], everyday light sources and solar cells. Furthermore they are used in broadband light-emitting diode (LED), memory elements, flexible displays, photodetectors.

We have to add that a lot of these applications are still developed in research institutions and are not yet available for commercial use.

Although the applications seem impressive and will probably motivate new technologies, there are reasonable concerns about these nanoscale particles. Some of the materials are toxic and through the small sizes it is unclear what might happen if the particles end up in living organisms or generally speaking, into the environment. For more interested readers, we recommend the following paper for further reading: **Hardman Hardman** [Hardman].

Chapter 2

Colloidal Nanocrystal Synthesis

The colloidal chemistry has offered a remarkable amount of tools for creating nanostructures. In the past growing simple, spherical, monodisperse NCs was the starting point of this research area, whereas nowadays various shapes, such as spheres, cubes, tetrapods, wires or rods can be engineered. The main advantages of the colloidal synthesis are:

- High precision shape control of the crystal and multicomponent structures
- Good size adjustability, through which the optical properties of the material are determined
- Monodispersity of the NC
- Low energy and low cost fabrication with a simple experimental setup
- Broad range of materials, including metals, semiconductors and magnetic materials can be synthesized at sub-20nm range

Due to the listed advantages, the colloidal NC synthesis is the best candidate for commercial applications so far.

Remark. In the following section, we will be use some chemical terms. Their meaning can be looked up in the glossary on page 22.

2.1 The synthesis

The colloidal NC synthesis is a wet chemical method to create nanostructures. It is based on a three-component system composed of precursors, organic surfactants and solvents. Its basic idea is the controlled growth of a NC, which is mainly depending on time.

The basic apparatus of the synthesis is given in figure 2.1. It shows a reaction flask with thermometer and injection in form of a syringe. In praxis a heater is installed around the lower part of the flask, to keep the solvent at a desired constant temperature. The procedure itself starts with the heating of a solvent funneled into the flask. The thermometer will indicate the temperature of the solvent, which is a key variable for a good growth process. Therefore it is important to control, as the reaction will have an influence on the temperature as well. Figure 2.1 furthermore illustrates the stages of the synthesis using the traditional LaMer model by the U.S.-American chemist Victor LaMer. The nucleation process starts after the injection of the precursors into the flask, where they decompose and form monomers, which will cause the nucleation and growth of the NCs. The size of the NC is at this stage primarily determined by the time, i.e. the longer the reaction, the larger the crystals will grow. The energy required to decompose the precursors is provided by the solvent in the flask, either by thermal collisions or by a chemical reaction between the liquid medium and the precursors or by a combination of these two mechanisms [Schmid]. Once monomer concentrations are sufficiently depleted, growth can proceed by Oswald ripening. Smaller particles combine with larger ones and cause therefore a lower concentration of particles in the solution. Unfortunately, the process is more complicated, as the model predicts. It does not hold for hot-injection schemes for instance, because nucleation, ripening and growth may almost occur concurrently [Klimov]. Furthermore the nucleation process does not have to start immediately after injection, but it is usually a single discrete event in time. In the following paragraph we will explain the variables that influence the reaction and their relationship to each other.

As soon as the final size is reached, the reaction is stopped, by switching off the heating and cooling down the compound. After the reaction is stopped, the NCs get washed to remove impurities from the reaction.

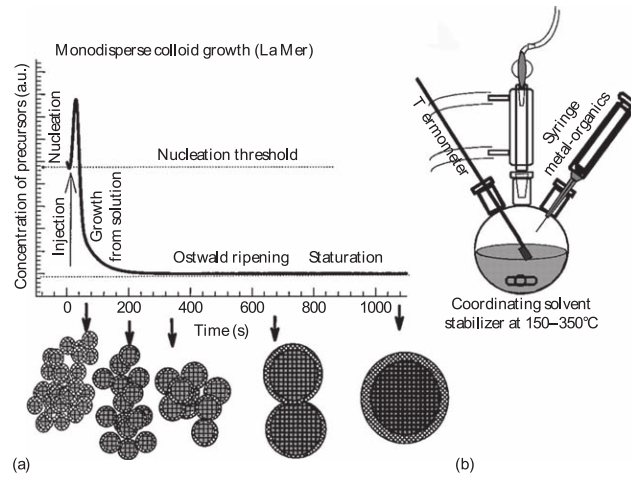


Figure 2.1: (a) Stages of the monodisperse NC synthesis according to La Mer. (b) Basic apparatus used in the synthesis. SOURCE: [Klimov]

2.2 Reaction conditions

Typically, finding the right conditions for a reaction is a very difficult task. For different materials, the conditions change and the reaction components have to be tailored exactly for this specific material. Hence finding an optimal set of conditions decides over the quality of the resulting NCs.

Duration of the particle growth As mentioned, the duration of the process after injecting the precursors, determines the size of the particles. One might ask, when the right moment is to stop the synthesis, because the particles itself cannot be measured during the reaction. Due to this fact, the time to reach a desired size is determined empirically.

Reaction temperature The temperature is a critical factor for determining optimal crystal growth. High reaction temperatures of 125°C-400°C are often needed to anneal out defects in the crystalline lattice to form highly crystalline particles [Schmid]. In addition to that precursors have to withstand such high temperatures on the one hand and on the other hand temperatures need to be high enough, that precursors turn into monomers. This contradiction makes researchers to look for specific materials that fit the needed conditions.

Concentration of surfactants The choice of surfactants varies from case to case: a molecule that binds too strongly to the surface of the QD is not suitable, as it would not allow the crystal to grow. On the other hand, a weakly coordinating molecule would yield large particles or aggregates.

The combination of these conditions decides, if the final QD is of poor or high quality. Especially for semiconductor QDs a high luminescence efficiency is of great importance, since one would like to use the NCs for example in solar cells. Therefore a high efficiency rate would increase the performance of the photovoltaic elements. This can be achieved by a proper control of surface chemistry, as this can eliminate midgap states associated with surface dangling bonds [Talapin].

Chapter 3

QD Solar Cells

This chapter gives a brief overview over the fundamental principles of photovoltaic cells and QD solar cells in particular, then focuses on the example of PbS cells to give some specific information.

3.1 Solar Cell Principles

The basic idea of a solar cell is to convert light into electrical power. Light is absorbed in a material, thus generating an electron-hole pair. The generated electrons and holes must then be separated and conducted to electrodes attached to the material. The accumulation of carriers at the electrodes generates a potential difference, and a current will flow between the electrodes, if a load is connected.

The carrier separation can be achieved by an electric field inside the material. Different types of solar cells exist, based on different approaches. The typical silicon solar cell uses a semiconductor p-n junction: When a photon (with energy greater than the band gap) is absorbed in the semiconductor, an electron is promoted from the valence to the conduction band. Near the junction, these photogenerated electrons and holes are swept away to different sides, due to the built-in electric field of the p-n junction (fig. 3.1).

Other approaches are also widely used, for example Schottky contacts (metal-semiconductor interface) or semiconductor-liquid interfaces.

The electrical behaviour of a photovoltaic cell can be well described by its I-V characteristics (fig. 3.2). In the dark, the cell behaves like a diode (in the case of a p-n junction solar cell this seems fairly obvious). Under illumination, the curve is shifted vertically downwards. It crosses now the fourth quadrant, where the electrical power $P = IV$ is negative, which indicates that power is delivered to the load.

To characterise the solar cell, there are some common parameters, which are mentioned in the following paragraph. The open-circuit voltage V_{OC} is the maximum voltage provided by the cell. It is directly related to the energy band structure and thus to the built-in potential. The short-circuit current I_{SC} gives the maximum current, which flows if the electrodes are connected. I_{SC} is proportional to the carrier density under illumination and to the carrier mobility, which are therefore important parameters to maximize.

An often used quantity is the *fill factor (FF)*, which is the ratio between the maximum power $P_M = I_M V_M$ and the product $I_{SC} V_{OC}$. It describes how well behaved the I-V characteristics are (the more the curve approaches a rectangular shape, the better).

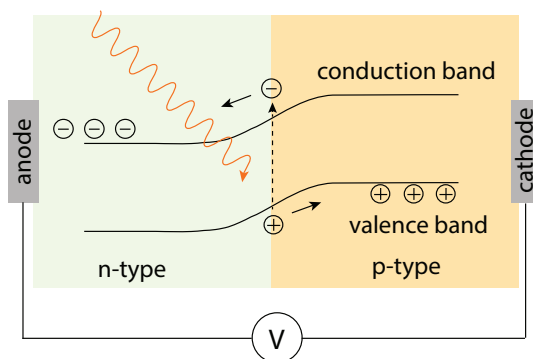


Figure 3.1: Principle of a solar cell using a p-n semiconductor junction.

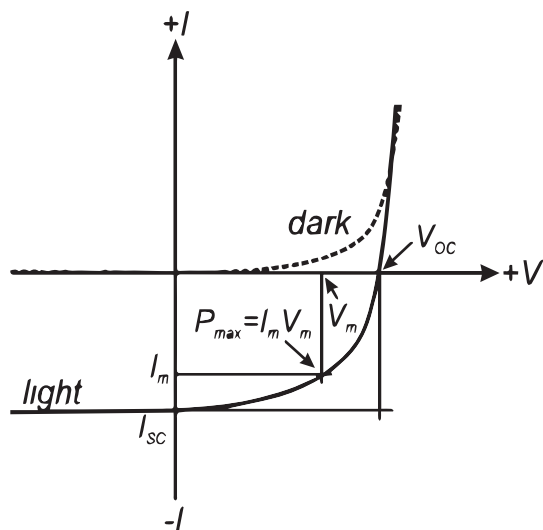


Figure 3.2: Typical I-V characteristics of a solar cell. SOURCE: [Talapin]

Of practical importance for comparing solar cells is the power conversion efficiency η , giving the ratio of optical power which is converted into electrical power.

$$\eta = \frac{P_{max}}{P_{in}} = FF \frac{I_{SC}V_{OC}}{P_{in}}$$

Usually an optical source called AM1.5 is used, whose spectral intensity distribution matches that of sunlight reaching the earth's surface at an angle of 48.2°. [Talapin]

3.2 Solar Cells using QDs

<<< HEAD Semiconductor nanocrystal solids, can be used for solar cells. Thus nanocrystals (NC) made of CdSe, CdTe, PbSe, PbS and many more can be used for this purpose. Like with bulk semiconductors, heterojunction solar cells are possible (using materials with different band gaps), such as CdSe-CdTe cells [Talapin]. Similarly, using Schottky-contacs is also an option.

=> Semiconductor nanocrystal solids can be used for solar cells. Thus nanocrystals (NC) made of CdSe, CdTe, PbSe, PbS and many more can be used for this purpose. Like with bulk semiconductors, heterojunction solar cells are possible (using materials with different band gaps), such as CdSe-CdTe cells [ChemRev]. Similarly, using Schottky-contacs is also an option.

>>> bcabdd6f940bd618ed317354202fe8b026b2551b

Using NC solids made of QDs offers several advantages. One big advantage is the possibility of choosing the size of the band gap by controlling the size of the QDs, which can be done easily during the synthesis of CQDs. Controlling the band gap means essentially choosing the spectrum which can be absorbed, and consequently cells, which can make use of a broad spectrum, can be engineered.

Furthermore QD solar cells are easy to fabricate and that at low costs. Large-scale production would also be possible [Talapin].

Using NC solids, there are promising perspectives for more advanced techniques, in order to increase efficiency. These involve e.g. carrier multiplication (the absorption of one highly energetic photon causes the creation of multiple electron-hole pairs) or hot carrier solar cells (electrons in higher energy states in the conduction band are extracted before they relax to the band edge and lose some energy).

However, there are some problems which have to be overcome. One is the (air-) stability and lifespan of QD based photovoltaic cells. In many cases, the devices lose dramatically in efficiency after some time, which can be as short as hours or even minutes [Tang2011]. Another problem is the currently rather low efficiency of the cells (maximum achieved efficiency of around 7% for a PbS cell [Ip2012]). One issue leading to reduced efficiency is the presence of undesired states in the band gap (mid-gap or trap states). These arise due to 'dangling' (unbound) bonds of surface atoms and are significant in a QD, since its surface to volume ratio is high. So-called *passivation* of the surface is thus very important.

Furthermore, for future large-scale production, the materials used in the production process should be cheap, available in large quantities and preferably non-toxic, which contrasts with some NC materials that contain toxic elements like Cd or Pb.

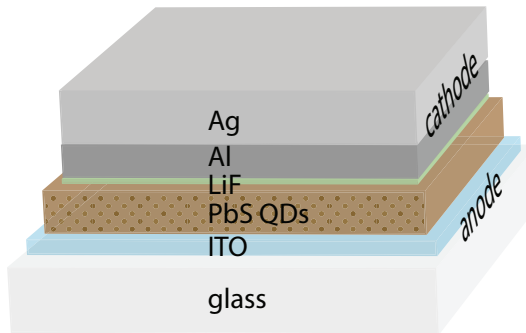


Figure 3.3: Structure of a PbS solar cell.

3.2.1 Example of a PbS QD Solar Cell

Since the structure and fabrication methods of QD solar cell are quite diverse, we will focus here on a PbS QD solar cell, as they were produced at ETH at the Laboratory for Nanoelectronics [MS _ Michael]. Due to the small band gap of PbS (0.37eV for bulk PbS), the solar cell is able to convert power from the near infrared spectrum. This is of interest, since roughly 50% of the solar energy that reaches the earth is in the infrared spectrum.

Structure

The principle part of the cell is a Schottky junction of PbS and Al, with a thin protection layer (1 nm) of LiF in between. The Schottky barrier is responsible for the electric field which separates the photogenerated carriers. The Al Cathode is covered by a layer of silver, for better air stability. The transparent anode is formed of a layer of indium tin oxide (ITO), on top of the PbS (fig. 3.3).

Fabrication Process

The main steps involved in the fabrication are described below, as they were carried out in reference [MS _ Michael].

We start with a glass substrate, which is coated with ITO using lithography. The sample has then to be cleaned (using solvents, and afterwards by O_2 plasma treatment to remove organic residuals).

In the next step, the active layer, i.e. the PbS QDs, is deposited. This can be done by dip coating, where the substrate is immersed in a PbS-hexane solution, and taken out after a few seconds, leaving a thin film of the solution on the sample. Alternatively, spin coating can be used, where several drops of the PbS-Hexane solution are dropped on the substrate, which is then rotated to spread the drops, leading to a film of homogeneous thickness.

Now the long ligands surrounding the QDs have to be exchanged for short ligands, in order to improve inter-particle coupling (and thus e.g. carrier mobility). For this purpose, the substrate is immersed into a suitable compound: Ethandithiol, benzenedithiol (both organic), and ammonium thiocyanate (NH_4SCN , inorganic) can be used.

The sample is then rinsed in acetonitrile and or hexane. In order to obtain a PbS film of desired thickness, the steps of spin (respectively dip) coating, ligand exchange and rinsing have to be repeated several times.

In a last step, the cathode, i.e. the three layers of LiF, Al and Ag are evaporated on the substrate.

Chapter 4

Analysis of PbS QD simulation data

In this chapter we will take a look at the simulation data, which are based on a tight-binding model used by OMEN . The parameters used for the simulation can be found in appendix A on page 21. We will make an analysis of the energy levels and wave functions of PbS QDs and draw some conclusions.

Remark. There are a few practical aspects to note concerning the simulation of PbS QDs with OMEN : Since OMEN will consider in its calculation 18 orbitals for the atoms, one must keep in mind that the simulation uses significantly more computing resources than a simulation of, for instance, a CdSe-CdS QD. Especially the memory usage during the calculation can easily exceed 10GB for larger QDs. The size of the generated simulation data for one QD can also amount to more than a few 100MB. It has to be kept in mind, that the number of atoms scales with the third potence of the radius. Another problem is the high degeneracy of energy levels. This makes it necessary to simulate a higher number of modes, thus increasing the usage of resources further.

4.1 Energy levels

Remark. In the following discussion, the terms conduction band, band edge and so on are used. Although there are no energy bands present in a QD, but rather discrete energy levels, these terms make sense nevertheless, since the states above the band gap are similar to conduction band states, and those below to valence band states, respectively. Indeed, if the QD gets bigger, we finally reach the limit where we can treat it as a bulk material. The term *conduction band* thus refers in this context to the discrete energy states above the band gap.

Taking a look at the eigenenergies close to the bandedge, one can see that there are 8 closely spaced modes, for conduction and valence band respectively. Generally, closest to the band edge there is a twofold degenerate energy level, followed by a fourfold degenerate level and then again a twofold degenerate level. (For a few simulations the order is different, e.g. the fourfold degenerate energy level may be closest to the

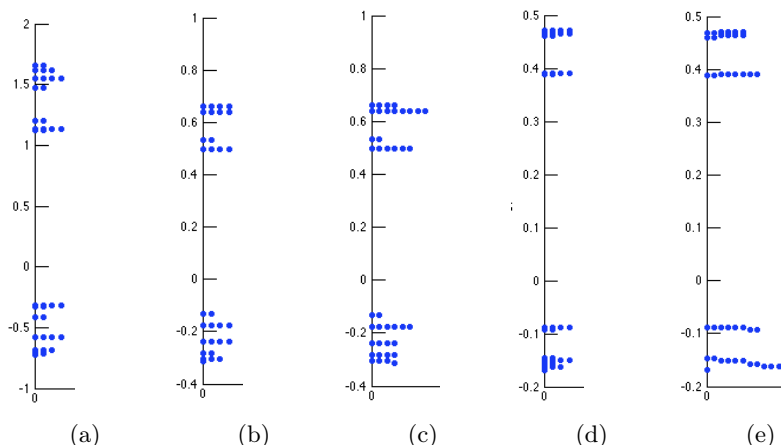


Figure 4.1: Energy levels for different sized QDs: 2nm (a), 6nm (b) and (c), 10nm (d) and (e). Vertical axis in eV. Multiple dots on the horizontal axis signify degeneracy. In plots (c) and (e) energies within 0.03eV are plotted as degenerate, for better visibility.

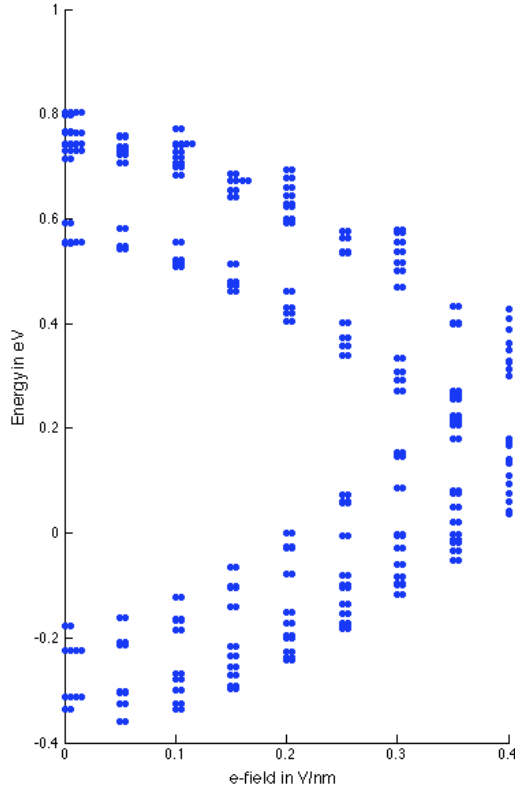


Figure 4.2: Energy states (including degeneracy) for different electric fields.

band edge.)

As the size of the QDs increases, the energy levels get closer to each other, resulting in higher degeneracy. This is shown in figure 4.1 (a),(b),(d), where the energy levels (including degeneracy) are shown for 2, 6 and 10nm QDs. Since some levels are very closely spaced, they are not clearly distinguishable from each other. For this reason, the tolerance, within which an energy level is shown as degenerate, was increased in figure 4.1 (c),(e). An effective eightfold degeneracy for the 10nm QD is now clearly visible.

<<< HEAD In the presence of an electric field, this degeneracy is broken, leading to more energy levels, which are all, interestingly, twofold degenerate. This is shown in figure 4.2 for a 5nm QD, where the energy levels are plotted against applied electric field. One can also clearly see how the band gap gets smaller, as is discussed later on. ===== In the presence of an electric field, this degeneracy is broken, leading to more energy levels, which are all, interestingly, twofold degenerate. This is shown in figure 4.2 for a 5nm QD, where the energy levels are plotted against applied electric field. One can also clearly see how the bandgap gets smaller, as will be discussed later on. >>> bcabdd6f940bd618ed317354202fe8b026b2551b

4.2 Band gap

All band gaps of our PbS simulations are plotted in figure 4.3. Furthermore, we have fitted the $1/R^2$ dependence of equation 1.1 to all band gaps where no voltage was applied. As we can see from the graph, the bulk band gap of lead sulfide (PbS) should approximately be 0.46eV, which means a pretty big deviation from experimentally determined values of 0.37eV at 302K (see appendix A). We have made the same observations while comparing other experimental with simulation data. As experimental data, transmission electron microscopy (TEM) images, absorption and PL spectra (see figure 4.4, 4.5 and 4.6) were available. From the TEM images, average particle sizes were measured and compared with approximately equivalently sizes from simulations. The results are listed in table 4.2. Significant deviations can be noticed between experimental and simulated data, which are reasoned in three significant error sources, that explain the deviations. First of all, the synthesis does not deliver perfect spherical and homogeneous QDs, which causes the broadening of the spectra. Second: it is very difficult to determine the size of the QDs from the TEM images, especially without sophisticated software. This might lead to comparison of experimental and simulated values, that actually do not belong to each other. Third: comparing measurements of the real physical world with simulations. There might be errors in the measurement apparatus, impurities in the QDs and disregarded effects in the simulation, which have an impact in reality.

Remark. All experimental data used in this section were provided by the Laboratory for Nanoelectronics (LNE) at ETH Zurich.

| | $\sim 2.97\text{nm} - 3\text{nm}$ PbS - 261 ¹ | $\sim 3.21\text{nm} - 3\text{nm}$ PbS - 61 | $\sim 3.95\text{nm} - 4\text{nm}$ PbS - 190 | $\sim 4.97\text{nm} - 5\text{nm}$ PbS - 220 |
|-----------------------|---|---|--|--|
| Energy at PL peak | 1.4529eV (853nm) | 1.2256eV (1012nm) | n/a | 1.0040eV (1235nm) |
| Band gap experimental | 1.7487eV (709nm) | 1.5194eV (816nm) | 1.2808eV (968nm) | 1.0489eV (1182nm) |
| Band gap simulated | 0.9929eV | 0.9929eV | 0.8645eV | 0.7296eV |

Table 4.2: Comparison of experimental and simulated band gaps.

4.2.1 Band gap of QDs in presence of an applied voltage

In figure ?? we see, that with increasing voltage the band gaps approach a zero value. Interestingly, this does not happen linearly, for every constant voltage increment. Visualizing this effect for constant radii (figure 4.7), we recognize that the energy gap drops in a parabolic way until it completely reaches the zero value. Furthermore, we recognize in figure 4.8 a shift of all energy levels towards each other.

4.3 Wave functions

4.3.1 Shape of the wave functions

QDs bigger than 3nm

Remark. Although the term *wave function* appears a lot in this section, the term is rather meant in the sense of *probability density*, since the plots, on which the analysis is based, are more easily interpreted if they show probabilities instead of complex numbers.

Sometimes, the wave functions of QDs are described in analogy to atomic orbitals, labeling them S, P, D and so on, with subscript e or h, denoting electron-like (conduction band) states or hole-like (valence band) states respectively. We will see how well this picture corresponds to the simulation.

The 8 energy states ('modes') closest to the band edge (for conduction and valence band respectively) have wave functions with spherical symmetry, where the highest probability density is in the center (fig. 4.9). This is in agreement with the 8 predicted $1S_{e,h}$ orbitals for PbS [Talapin].

The higher energy states show wave functions with more complex shapes. For example, a 8nm QD shows the following wave function shapes: After the 8 spherical conduction band states follow 4 (degenerate) states with barbell shape, in different orientations. Then 2 states with spherical shell shape. After that, 2 states with a shape similar to two crossed barbells, then again 2 spherical shell-like states, followed by 2 ring-shaped wave functions, and so on (fig. 4.10). For the valence band states, the shapes are similar, although they do not occur in the same order (the same is true for QDs of different sizes).

QDs smaller than 3nm

<<< HEAD For QDs smaller than 3nm, the problem is that it is more difficult to see the shape of the wave function (too few atoms). Furthermore it is not clear how well this models a real QD, since the surface (and thus passivation of the surface) begins to have an even bigger influence.

For a 2 and 3nm QDs, the 8 lowest conduction band states still remain more or less spherical. Whereas the valence band states start lose spherical symmetry. For a 3nm QD, mode 7 and 8 are already slightly asymmetric (fig. 4.11 (a)), and for the 2nm QD, even the modes 1 to 4 are clearly not spherical, but the wave function is rather localized at two sides (fig. 4.11 (b)). ===== For QDs smaller than 3nm, it is more difficult to see the shape of the wave function (too few atoms). Furthermore it is not clear how well this models a real QD, since the surface (and thus passivation of the surface) begins to have an even bigger influence.

For a 2 and 3nm QDs, the 8 lowest conduction band states still remain more or less spherical, whereas the valence band states start lose spherical symmetry. For a 3nm QD, mode 7 and 8 are already slightly asymmetric (fig. 4.11 (a)), and for the 2nm QD, even the modes 1 to 4 are clearly not spherical, but the wave function is rather localised at two sides (fig. 4.11 (b)). >>> bcabdd6f940bd618ed317354202fe8b026b2551b

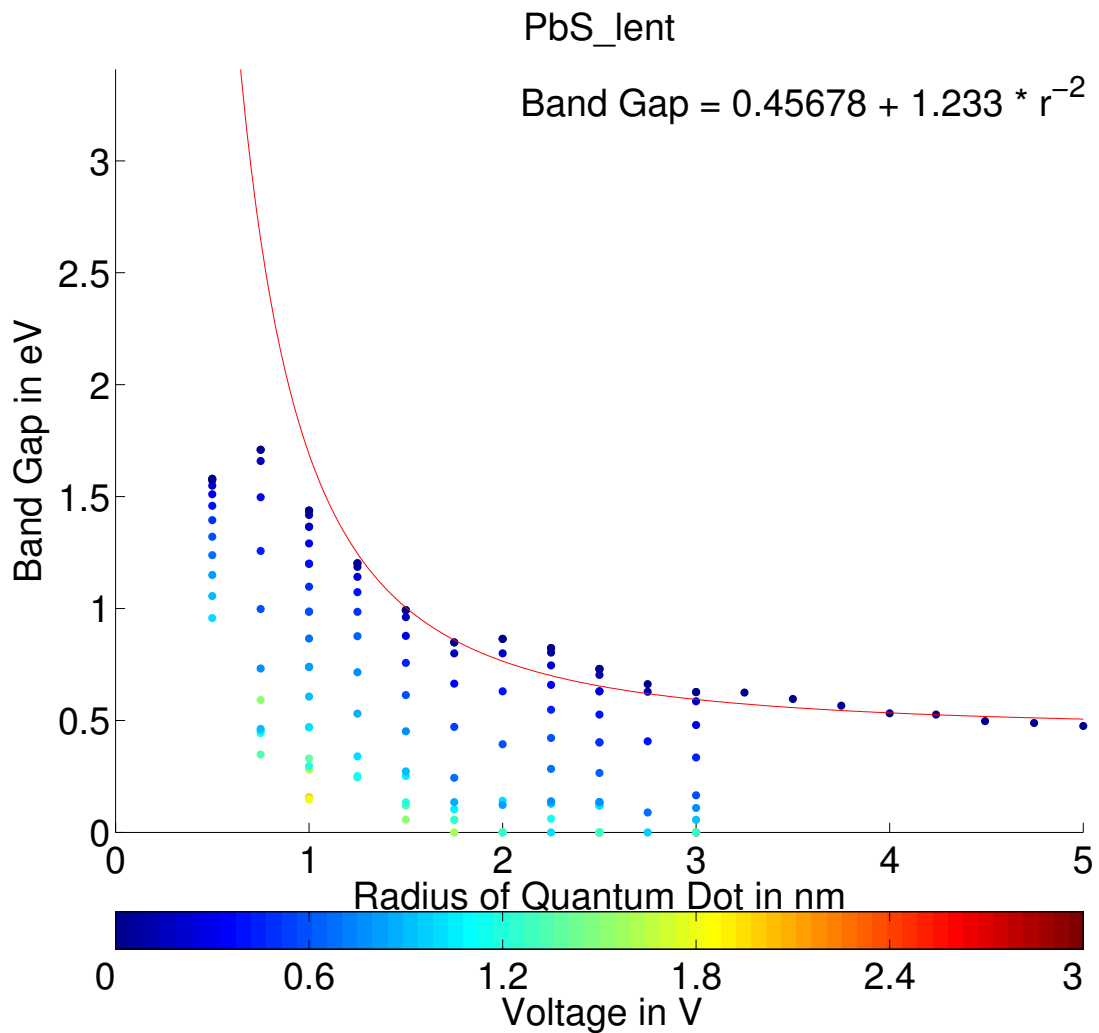


Figure 4.3: PbS band gaps against radius of all simulated QDs. The color indicates the applied voltage.

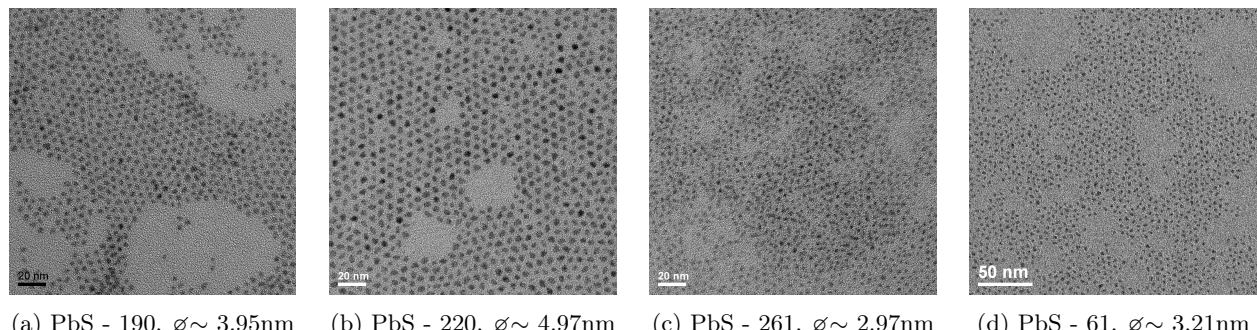
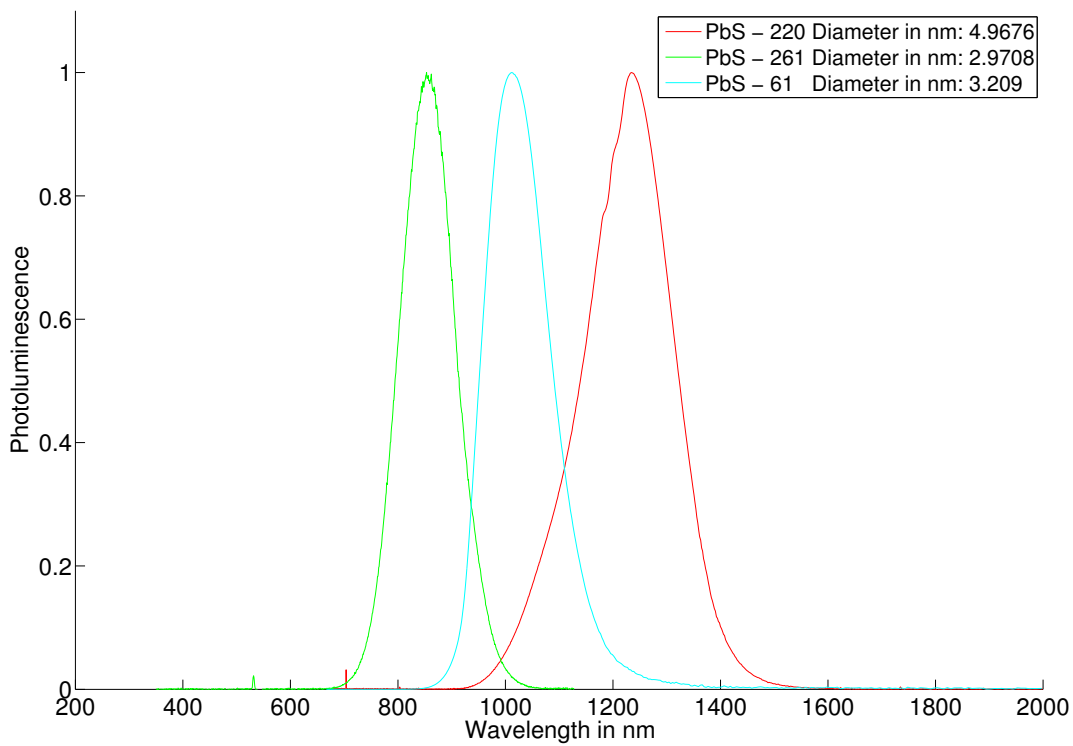
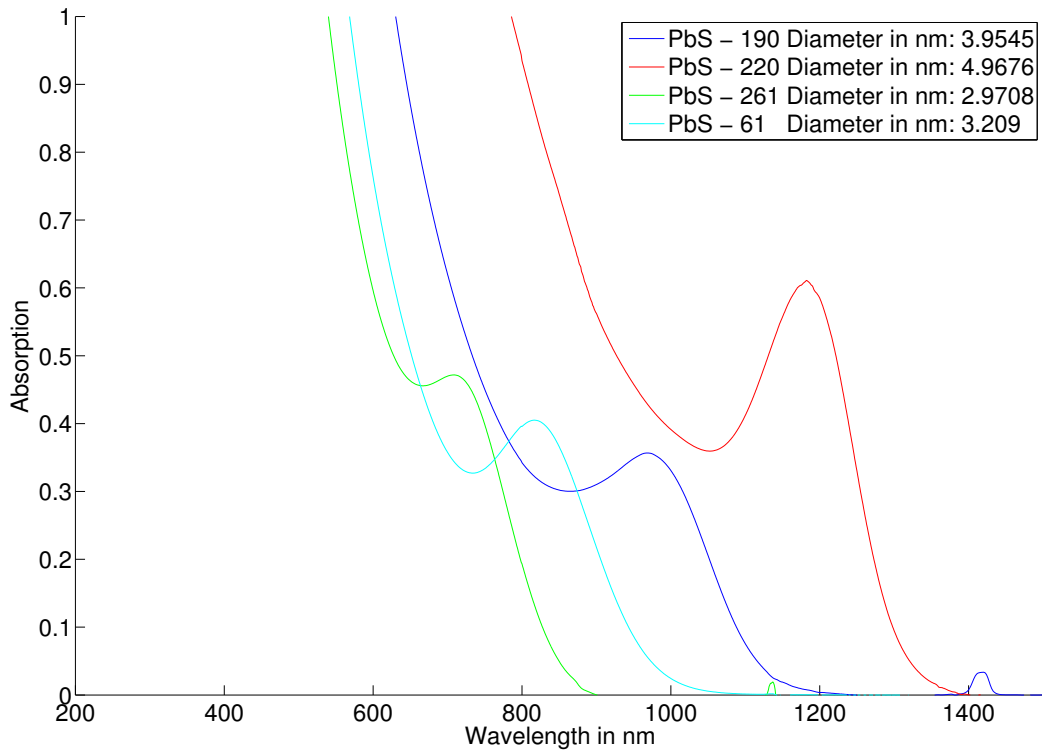


Figure 4.4: TEM images of PbS QDs



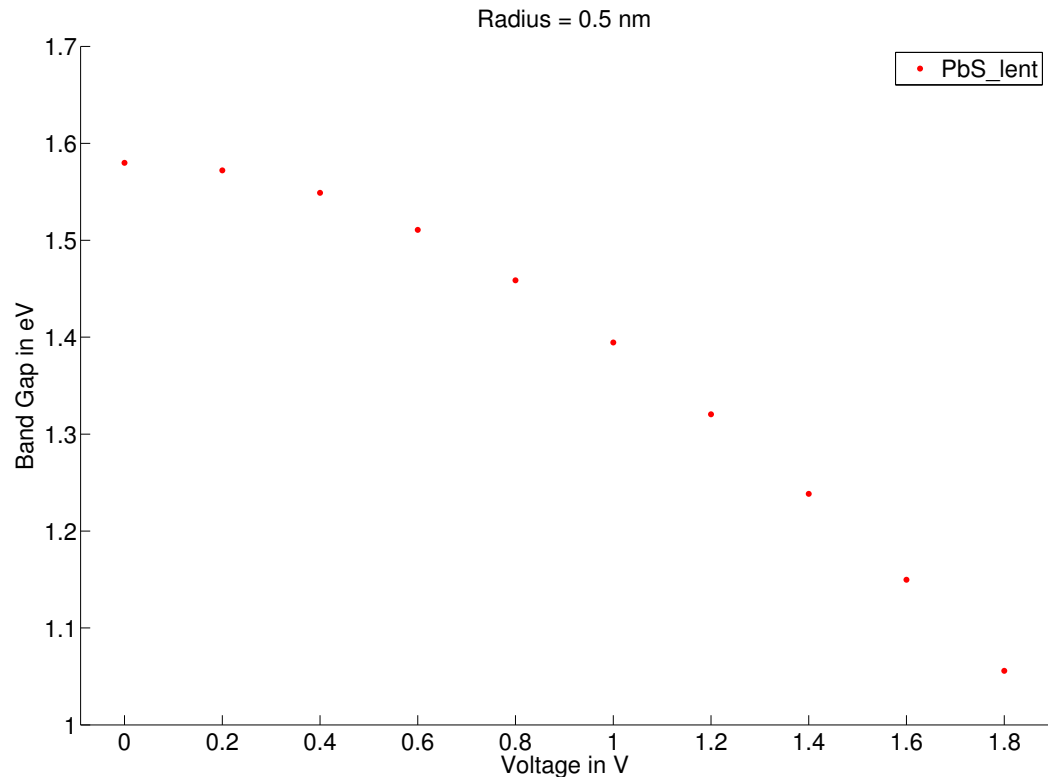


Figure 4.7: PbS band gaps plotted against voltage with constant radius 0.5nm.

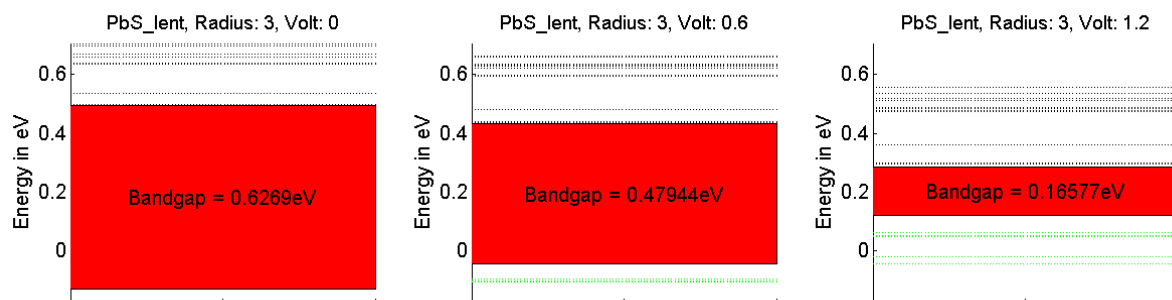


Figure 4.8: PbS energy levels for different voltages with constant radius 3nm.

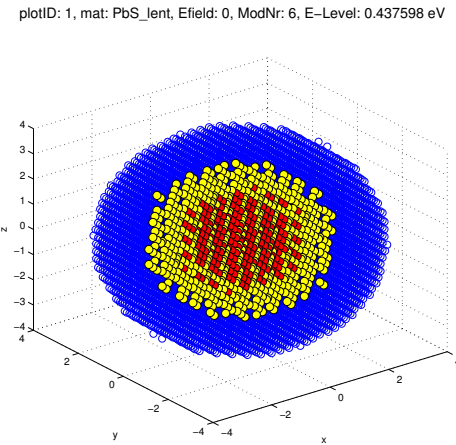


Figure 4.9: Probability density for an energy state in the lower conduction band of an 8nm QD. Locations of very high probability are shown in red, those of medium to high probability in yellow, such that the sum of the probabilities of all yellow and red locations is 50%. Note: In figures later on, different probability values may be used for better visibility.

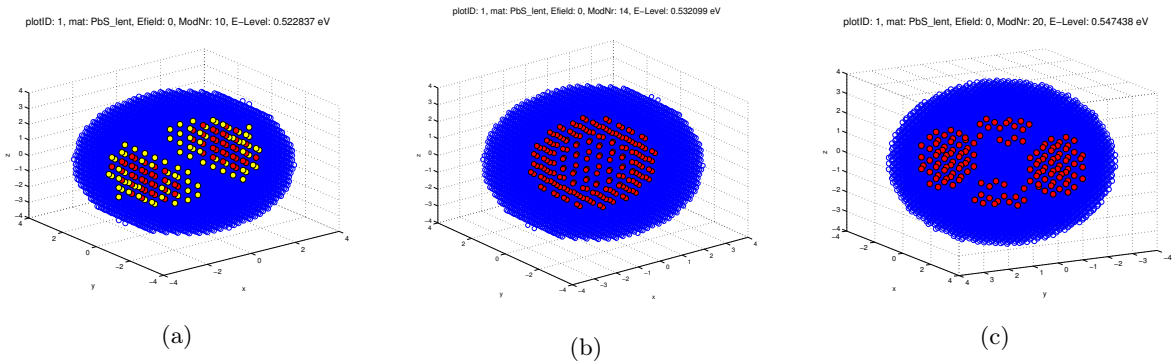


Figure 4.10: Probability density for higher energy states in an 8nm QD: barbell-shape (a), spherical shell-shape (b), crossed barbell-shape (c). In plots (b) and (c) the locations of medium high probability (yellow points) are not shown for clarity.

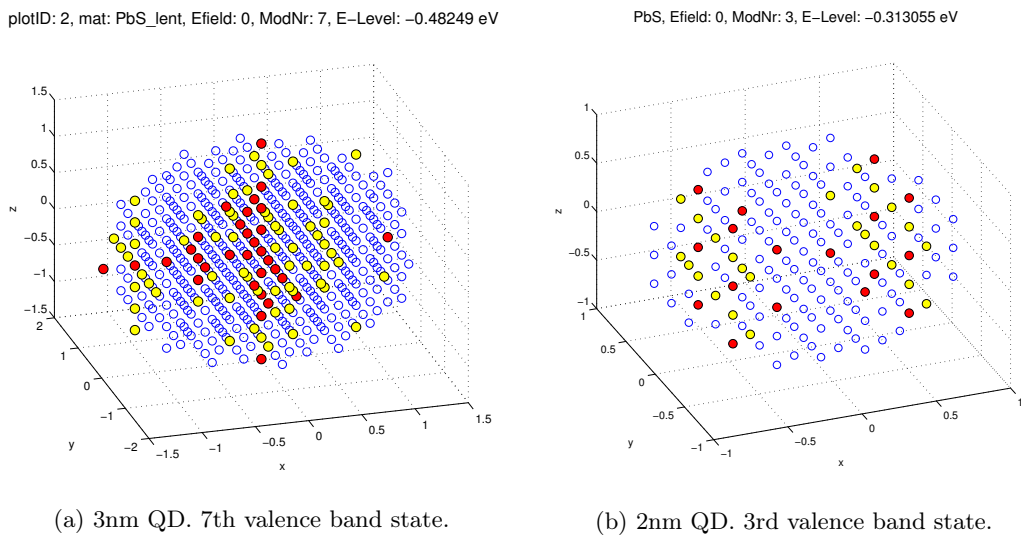


Figure 4.11: Probability density for valence band states. The shapes start to lose spherical symmetry.

4.3.2 Influence of an electric field

The presence of an electric field results in a shift of the wave function, i.e. the maximum of the probability density is not in the center anymore and the spherical symmetry of the 8 first states is broken (for conduction and valence band respectively). Furthermore, one can see that the valence band states really behave differently than conduction band states: The wave function is shifted in the opposite direction (fig. 4.12). This confirms that the valence band states are hole-like, similar to bulk semiconductor band theory.

««< HEAD For larger electric fields the band gap gets smaller, until it finally disappears, i.e. conduction and valence band states are not separated anymore. For example, for a 5nm QD, the band gap disappears for electric fields larger than 0.35 V/nm (fig. 4.2). The states close to the (former) band gap cannot be separated in conduction and valence band: as energy increases, some hole-like states are followed by electron-like (i.e. conduction band-like) states, which in turn are followed by hole-like states and later again electron-like states (fig. 4.13).

Additionally, with higher electric fields, the wave functions seem not only to be shifted, but change shape: Some now look more like asymmetric barbells or even stranger, ring-like shapes (fig. 4.13 (a) and (f)). ===== For larger electric fields the bandgap gets smaller, until it finally disappears, i.e. conduction and valence band states are not separated anymore. For example, for a 5nm QD, the band gap disappears for electric fields larger than 0.35 V/nm (fig. 4.2). The states close to the (former) band gap cannot be separated in conduction and valence band: as energy increases, some hole-like states are followed by electron-like (i.e. conduction band-like) states, which in turn are followed by hole-like states and later again electron-like states (fig. 4.13).

Additionally, with higher electric fields, the wave functions seem not only to be shifted, but change shape: Some now look more like asymmetric barbells or even stranger ring-like shapes (fig. 4.13 (a) and (f)). »»> bcabdd6f940bd618ed317354202fe8b026b2551b

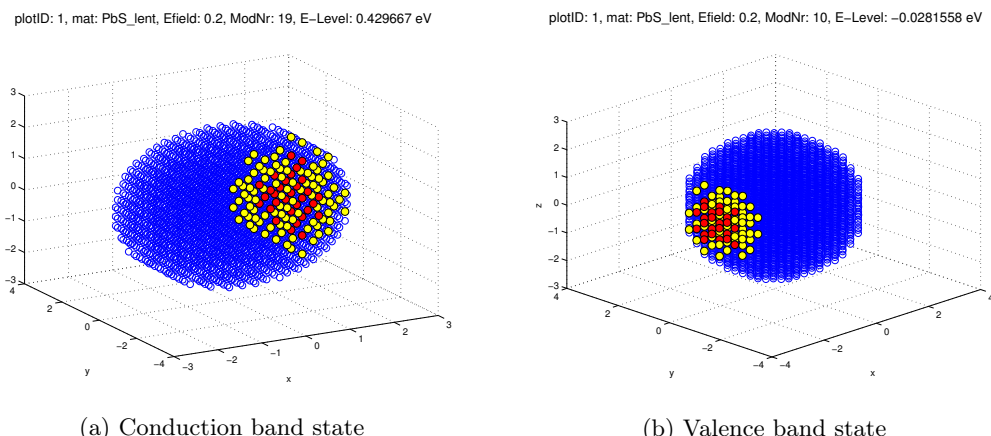


Figure 4.12: Probability densities for a 5nm QD in an electric field of 0.2V/nm.

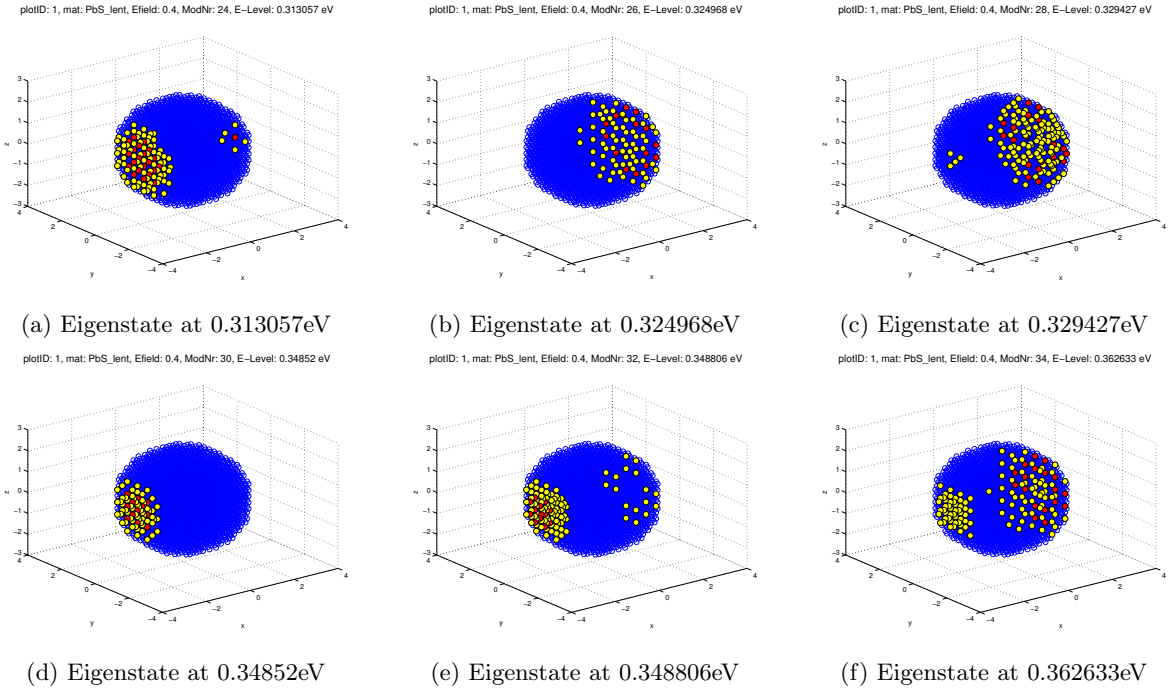


Figure 4.13: Probability densities in the presence of a high electric field (0.4V/nm). Increasing energy from (a) to (f). Hole-like states (a),(d),(e) become mixed with electron-like states (b),(c),(f).

4.4 Conclusions

We have seen that larger PbS QDs have eightfold degenerate energy states at the band edges, whose wave functions have spherical symmetry. Higher energy states show more complex wave functions. For QDs smaller than 3nm, the eightfold degeneracy is lost more and more, as well as the spherical symmetry of these wave functions. However, it is questionable how close to reality the simulations of very small structures below 2nm are. Under the influence of an electric field, the wave functions shift, according to their being hole- or electron-like, in opposite directions.

Furthermore we noticed, that the band gap is depending on size and the applied voltage. Increasing the voltage energy levels get closer with and cause a narrowing of the band gap.

Appendix A

Lead sulfide (PbS) parameters

A.1 Basic characteristics

Lead sulfide is an inorganic compound.

| | |
|---------------------|-----------------|
| Molecular formula | PbS |
| Molar mass | 239.30 g/mol |
| Density | 7.60 g/cm |
| Melting point | 1118°C, 1371 K |
| Boiling point | 1281°C, 1554 K |
| Index of refraction | 3.91 |
| Crystal structure | rocksalt |
| Lattice constant | 5.936 Angstrom |
| Energy gap | 0.37 eV at 302K |

Table A.1: Properties of PbS

A.2 Tight binding parameters

Our simulations are based on tight binding parameters determined by Craig S. Lent et al. in year **Lent1986** [[Lent1986](#)].

| | | | | | | | | | | |
|-------------|-------------|-----------|-----------|--------------|-----------|--------------|-----------|--------------|-----------|-----------------|
| $E_{s,c}$ | $E_{s,a}$ | $E_{p,c}$ | $E_{p,a}$ | $E_{d,c}$ | $E_{d,a}$ | | | | | |
| -6.546 | -13.827 | 3.486 | -1.153 | 9.27 | 10.38 | | | | | |
| λ_c | λ_a | | | | | | | | | |
| 1.559 | -0.211 | | | | | | | | | |
| $V_{s,s}$ | $V_{s,p}$ | $V_{p,s}$ | $V_{p,p}$ | $V_{p,p\pi}$ | $V_{p,d}$ | $V_{p,d\pi}$ | $V_{d,p}$ | $V_{d,p\pi}$ | $V_{d,d}$ | $V_{d,d\delta}$ |
| -0.364 | 0.936 | 0.186 | 2.073 | -0.281 | -1.142 | 1.16 | -1.54 | 0.517 | -1.67 | 0.659 |

Table A.2: Nearest-neighbor tight-binding parameters of PbS in eV

Declaration of Originality

We hereby declare that the written work we have submitted entitled

Simulation of Quantum Dots

is original work which we alone have authored and which is written in our own words.

Authors

| LAST NAME | FIRST NAME |
|------------|------------|
| Dittberner | Matthias |
| Funck | Christian |

Supervisors

| LAST NAME | FIRST NAME | DEGREE |
|-----------|------------|-----------|
| Luisier | Mathieu | Professor |
| Wood | Vanessa | Professor |

With the signature we declare that we have been informed regarding normal academic citation rules and that we have read and understood the information on *Citation etiquette* (http://www.ethz.ch/students/exams/plagiarism_s_en.pdf). The citation conventions usual to the discipline in question here have been respected. The above written work may be tested electronically for plagiarism.¹

Place and date

Christian Funck

Place and date

Matthias Dittberner

¹Based on the official Declaration of ETH Zurich: http://www.ethz.ch/faculty/exams/plagiarism/confirmation_en.pdf